The very high X-ray polarisation of accreting black hole IGR J17091-3624 in the hard state

Melissa Ewing[©], ¹* Maxime Parra[©], ² Guglielmo Mastroserio[©], ³ Alexandra Veledina[©], ^{4,5} Adam Ingram[©], ¹ Michal Dovčiak[©], ⁶ Javier A. García[©], ^{7,8} Thomas D. Russell[©], ⁹ Maria C. Baglio[©], ¹⁰ Juri Poutanen[©], ⁴ Oluwashina Adegoke, ⁸ Stefano Bianchi[©], ¹¹ Fiamma Capitanio[©], ¹² Riley Connors, ¹³ Melania Del Santo[©], ⁹ Barbara De Marco[©], ¹⁴ María Díaz Trigo[©], ¹⁵ Poshak Gandhi, ¹⁶ Maitrayee Gupta[©], ⁶ Chulsoo Kang, ² Elias Kammoun[®], ⁸ Vladislav Loktev[©], ^{4,17} Lorenzo Marra[©], ¹² Giorgio Matt[©], ¹¹ Edward Nathan, ⁸ [©] Pierre-Olivier Petrucci[©], ¹⁸ Megumi Shidatsu[©], ² James F. Steiner[©], ¹⁹ Francesco Tombesi[©], ^{20,21,22} and Federico M. Vincentelli, ¹⁶

¹School of Mathematics, Statistics, and Physics, Newcastle University, Newcastle upon Tyne, NE1 7RU, UK

Accepted XXX. Received YYY; in original form ZZZ

ABSTRACT

We report the first detection of the X-ray polarisation of the transient black hole X-ray binary IGR J17091–3624 taken with the *Imaging X-ray polarimetry Explorer (IXPE)* in March 2025, and present the results of an X-ray spectro-polarimetric analysis. The polarisation was measured in the 2–8 keV band with 5.2σ statistical confidence. We report a polarisation degree (PD) of 9.1 ± 1.6 per cent and a polarisation angle of $83^{\circ} \pm 5^{\circ}$ (errors are 1σ confidence). There is a hint of a positive correlation of PD with energy that is not statistically significant. We report that the source is in the corona-dominated hard state, which is confirmed by a hard power-law dominated spectrum with weak reflection features and the presence of a Type-C quasi-periodic oscillation at ~ 0.2 Hz. The orientation of the emitted radio jet is not known, and so we are unable to compare it with the direction of X-ray polarization, but we predict the two to be parallel if the geometry is similar to that in Cygnus X-1 and Swift J1727.8-1613, the two hard state black hole binaries previously observed by *IXPE*. In the Comptonisation scenario, the high observed PD requires a very favourable geometry of the corona, a high inclination angle (supported by the presence of a dip in the light curve) and possibly a mildly relativistic outflow and/or scattering in an optically thick wind.

Key words: accretion, accretion discs - polarization - stars: black holes - X-ray binaries

1 INTRODUCTION

²Department of Physics, Ehime University, 2-5, Bunkyocho, Matsuyama, Ehime 790-8577, Japan

³Dipartimento di Fisica, Università degli Studi di Milano, Via Celoria 16, I-20133 Milano, Italy

⁴Department of Physics and Astronomy, 20014 University of Turku, Finland

⁵Nordita, KTH Royal Institute of Technology and Stockholm University, Hannes Alfvéns väg 12, SE-10691 Stockholm, Sweden

⁶Astronomical Institute of the Czech Academy of Sciences, Boční II 1401, 14100 Praha, Czech Republic;

⁷ NASA Goddard Space Flight Center, Greenbelt, MD 20771, USA

⁸ Cahill Center for Astrophysics, California Institute of Technology, 1216 East California Boulevard, Pasadena, CA 91125, USA

⁹INAF, Istituto di Astrofisica Spaziale e Fisica Cosmica, Via U. La Malfa 153, I-90146 Palermo, Italy

¹⁰INAF-Osservatorio Astronomico di Brera, Via Bianchi 46, I-23807 Merate (LC), Italy

¹¹ Dipartimento di Matematica e Fisica, Università degli Studi Roma Tre, Via della Vasca Navale 84, 00146 Roma, Italy

¹² INAF - IAPS, via del fosso del Cavaliere 100, 00133 Roma, Italy

¹³ Department of Physics, Villanova University, 800 E. Lancaster Avenue, Villanova, PA 19085, USA

¹⁴ Departament de Fisíca, EEBE, Universitat Politècnica de Catalunya, Av. Eduard Maristany 16, 08019 Barcelona, Spain

¹⁵ ESO, Karl-Schwarzschild-Strasse 2, 85748, Garching bei München, Germany

¹⁶ School of Physics & Astronomy, University of Southampton, Southampton SO17 1BJ, UK

¹⁷Department of Physics, P.O. Box 64, 00014 University of Helsinki, Finland;

¹⁸Université Grenoble Alpes, CNRS, IPAG, 38000 Grenoble, France

¹⁹ Center for Astrophysics | Harvard & Smithsonian, 60 Garden St, Cambridge, MA 02138, USA

²⁰ Physics Department, Tor Vergata University of Rome, Via della Ricerca Scientifica 1, 00133 Rome, Italy

²¹ INAF – Astronomical Observatory of Rome, Via Frascati 33, 00040 Monte Porzio Catone, Italy

²² INFN - Rome Tor Vergata, Via della Ricerca Scientifica 1, 00133 Rome, Italy

tremely high X-ray flux. They are categorised into transient or persistent systems, where transient systems exhibit outbursts followed by quiescence and persistent systems maintain a steady flux above a quiescent level. In both cases we observe spectral state transitions (Fender et al. 2004; Done et al. 2007; Belloni 2010). In transient systems, the outburst begins in the hard state, which is dominated by the Comptonisation of photons from a quasi-thermal accretion disc (Shakura & Sunyaev 1973; Novikov & Thorne 1973) or internal synchrotron photons (Poutanen & Vurm 2009; Malzac & Belmont 2009; Veledina et al. 2011) in a hot cloud of electrons known as the 'corona' (Sunyaev & Titarchuk 1985). A steady compact jet is launched from the system during the hard state. The system then transitions through the intermediate state, where both the disc and corona are prominently observed in the spectrum, to the soft state, where now the spectrum is dominated by the disc and the compact jet is quenched. Again transitioning through intermediate states, the source moves back to the hard state and then quiescence. In the case of persistent sources, we observe these spectral transitions without the flux dropping to quiescence.

Because XRBs cannot be spatially resolved, the geometry and position with respect to the disc of the hard X-ray corona is still a matter of debate (Poutanen et al. 2018). Several models have been proposed such as the 'sandwich' model, whereby the corona is powered by energy dissipation above and below the disc (Haardt & Maraschi 1993; Svensson & Zdziarski 1994), the 'magnetic flare' model (Galeev et al. 1979; Beloborodov 1999) with the localised energy dissipation regions above the disc, the 'jet-base' model (Markoff et al. 2005) in which the corona is vertically extended at the base of the jet, the 'lamppost' model (Matt 1993) where a compact corona lies above the BH on its spin axis, and the 'truncated disc' model (Eardley et al. 1975; Esin et al. 1997; Poutanen et al. 1997) whereby the disc evaporates beyond a truncation radius into a large scale-height hot flow. Each of these models can produce the same spectra, and so it is vital that we collect more information on these systems in order to break this degeneracy.

With the launch of the *Imaging X-ray Polarimetry Explorer (IXPE*; Weisskopf et al. 2022), we now have access to linear X-ray polarisation information in the 2–8 keV energy range. We can measure the polarisation degree (PD) – the extent to which the source X-ray photons have aligned electromagnetic fields – and the polarisation angle (PA) – the angle at which the electromagnetic fields align. The PD increases with asymmetry of the emission region; i.e. with larger (more edge-on) inclination and smaller aspect ratio (Schnittman & Krolik 2010; Ursini et al. 2021; Poutanen et al. 2023). For Comptonised radiation, the PA aligns perpendicular to the major axis of the scattering region (i.e. the corona). This happens because photons scatter preferentially in the plane perpendicular to their polarisation vector, and they experience more scatterings along the major axis due to its higher scattering optical depth (Sunyaev & Titarchuk 1985; Ursini et al. 2021; Ingram et al. 2023).

The first BH XRB observed by *IXPE* during a hard state was Cygnus X-1 (hereafter Cyg X-1), the brightest persistent BH XRB observed in the sky. Linear polarisation was detected with a > 20σ statistical confidence, with PD = 4.0 ± 0.2 per cent and PA = $-20^{\circ}.7\pm1^{\circ}.4$ (Krawczynski et al. 2022). The PA was found to align with the direction of the radio jet, suggesting that the corona is perpendicular to the jet and elongated in the disc plane. This favours horizontally extended models such as the truncated disc model over those vertically extended, such as the lamppost or jet-base model. With a relatively low inclination angle of $i = 27^{\circ}.5\pm0^{\circ}.8$ inferred from optical observations of the binary (Miller-Jones et al. 2021), a low PD of ≈ 1 per cent was expected (Krawczynski & Beheshtipour 2022). One explanation

of this high observed PD is that the corona is more inclined than the binary system. This could be due to a misalignment between the BH and binary spin axes giving rise to a warped disc. Another potential explanation is an outflowing corona; Poutanen et al. (2023) showed that a mildly relativistic bulk coronal electron velocity of $v \sim 0.4\ c$ can boost the PD to the observed value for an aligned system (see also Dexter & Begelman 2024). If the former model is true, then this suggests that a significant subset of observed systems will exhibit a low PD. If the latter is true, then this implies that a high PD is common in XRB systems observed in the hard state.

The second BH XRB observed by *IXPE* in the hard state was Swift J1727.8–1613, a transient source that was discovered after going into a bright outburst in 2023 (Veledina et al. 2023). Again it was found that the PD was \approx 4 per cent and that the PA was aligned with the orientation of the radio jet (Wood et al. 2024). This outburst was the first time that X-ray polarisation had been tracked across a hard to soft state transition, where the PD was found to slowly decrease across the transition and the PA stayed constant (Ingram et al. 2024). The PD was later seen to reduce dramatically in the soft state (Svoboda et al. 2024), before recovering to the same level as before in the reverse soft to hard state transition (Podgorný et al. 2024).

IXPE observations of Type-1 Active Galactic Nuclei (AGNs) may also help constrain the properties of the X-ray corona, since current understanding suggests that the hard X-rays produced by AGNs originate from a corona similar to that found in X-ray binaries. The PA measurements of NGC 4151 (Gianolli et al. 2023, 2024), IC 4329A (Ingram et al. 2023) and MCG-05-23-16 (Marinucci et al. 2022) have been found to align with the radio jet or ionisation cone, suggesting again that the corona is extended in the disc plane. The observed PD values are also rather high (\sim 3 per cent for IC 4329A and \sim 5 per cent for NGC 4151), given that Type-1 AGNs are thought to be viewed from a fairly low inclination according to the unification scheme.

IGR J17091-3624 is a transient BH XRB first discovered in 2003 by INTEGRAL (Kuulkers et al. 2003), and is of particular interest due to its extraordinary variability behaviour. While IGR J17091-3624 exhibits all the spectral states of a typical XRB (Capitanio et al. 2012), it also displays 10 different exotic variability states (Altamirano et al. 2011; Court et al. 2017; Capitanio et al. 2012; Wang et al. 2024). This makes it one of two systems known to exhibit this behaviour, the other source being GRS 1915+105, which has exhibited 14 different variability states (Belloni et al. 2000), 7 of which in common with IGR J17091-3624, including a heartbeat-like pattern (Wang et al. 2024). These variability states were first hypothesised from observations of GRS 1915+105 as radiation pressure instabilities deriving from its high-Eddington accretion rates, but because IGR J17091-3624 has demonstrated the same variability states at a flux estimated to be $\sim 20-30$ times lower, this model is now being questioned. For example, the presence of substantial wind outflows from the accretion disk might significantly influence these instability patterns, potentially stabilizing or suppressing the observed heartbeat oscillations (Janiuk et al. 2015).

Here we report the results of the *IXPE* observation of IGR J17091–3624 in the hard state, taken in March 2025. We also discuss two shorter simultaneous observations by the *Nuclear Spectroscopic Telescope ARray (NuSTAR)*. In Section 2, we detail the data reduction procedure. In Section 3, we present the polarimetric analysis as well as spectro-polarimetric fits. In Section 4 we discuss our results and in Section 5 we summarise our conclusions.

2 OBSERVATION AND DATA REDUCTION

2.1 IXPE data

IGR J17091–3624 was observed by *IXPE* on 2025 March 7–10 for a total elapsed time of ~ 300 ks (obsID: 0450201). We measured a mean count rate of ~ 1 count s⁻¹ with a useful exposure time of ~ 160 ks.

IXPE is a joint NASA/Italian Space Agency mission launched on 2021 December 9 from the Kennedy Space Center. It consists of three identical gas pixel detector units (DUs) that record the spatial, energy, timing, and polarimetric information from each event within a 2–8 keV energy band. Specifications and observatory details can be found in Weisskopf et al. (2022).

We downloaded the cleaned Level 2 event files for each DU (Costa et al. 2001) from the High Energy Astrophysics Science Archive Research Center (HEASARC¹). We used ds9 to define a circular source region centred on the source with a radius of 60", and a background region of an annulus centred on the source with an inner radius of 150" and an outer radius of 300". Using the latest version of ix-PEOBSSIM (v31.0.3; Baldini et al. 2022) we used the xpselect tool to create source and background fits files filtered for these regions. For our model-independent analysis, we used the pcube algorithm to calculate the Stokes parameters for the source and background regions, and subtract the background Stokes parameters from the source. For the spectro-polarimetric analysis, we used the PHA algorithm to extract Stokes I, Q and U as a function of energy channel for the source and background region of each detector unit, employing the most recent calibration database files associated with the latest version of IXPEOBSSIM, using an energy bin width of 0.016 keV. Throughout our analysis, we do not employ track weightings, and the PA is defined as East of North.

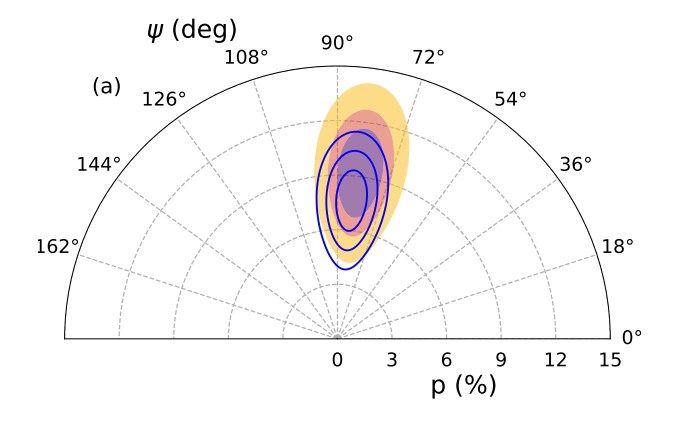
2.2 NuSTAR data

NuSTAR (Harrison et al. 2013) observed the source twice during the IXPE exposure (obsID 81002342008 and 81002342010). The observations started on 2025 March 7 at 14:00 UTC and on March 8 at 23:30 UTC, respectively, and each had a 20 ks exposure time. We used the nupipeline and nuproducts routines distributed from the NuSTARDAS v2.1.4 release with the calibration files 20250310 to produce the event files and the energy spectra for both Focal Plane Modules (FPMs). We chose an extraction region of 100" centred on the peak of the source photon counts. The same size region positioned as close as possible to the source was chosen for the background extraction. After preliminary analysis suggested that the spectra were broadly consistent between the two observations, we combined the FPMA and FPMB spectra from the two observations, as well as their backgrounds and response files, using addascaspec from the FTOOLS package. This was done to increase the signal for plotting purposes only. For a detailed analysis, it is best to treat the different observations and FPMs separately.

3 RESULTS

3.1 Model-independent analysis

We first measured the 2–8 keV polarisation using the IXPEOBSSIM algorithm pcube. We found PD = 9.1 ± 1.6 per cent and PA = $83^{\circ}\pm5^{\circ}$



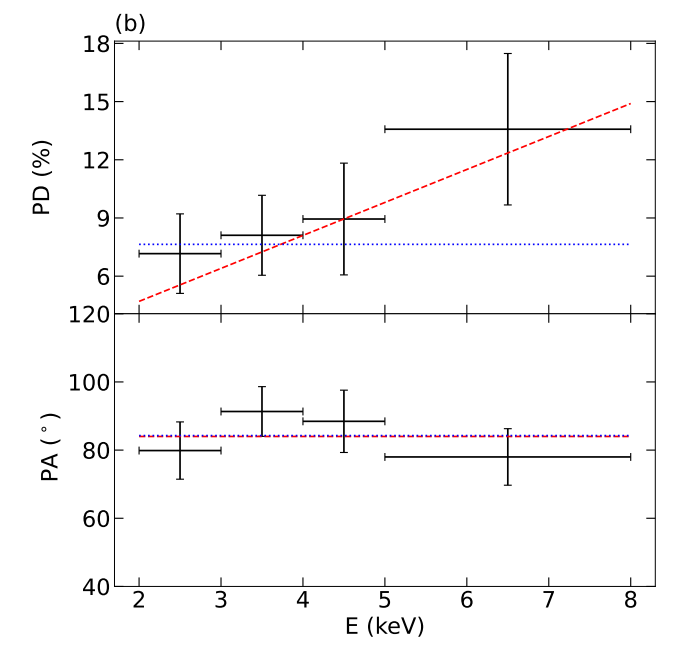


Figure 1. Polarimetric properties of IGR J17091–3624. (a) Constraints on the PD and PA (measured East of North) in the 2–8 keV band. The contours represent the confidence levels at 68, 90 and 99 per cent. The filled colour contours are the results of the unweighted, model-independent pcube algorithm. The blue contours are the results of an unweighted spectro-polarimetric analysis within xspec. (b) Energy dependence of the observed PD (top) and PA (bottom) with 1σ error bars as measured by the pcube algorithm. The red dashed lines represent the best-fitting energy dependent spectro-polarimetric model (row 4 of Table 1), where the PD increases with energy while the PA remains constant. The blue dashed lines represent the best fitting constant polarisation model.

 $(1\sigma$ uncertainties), and we plot the statistical confidence contours in Fig. 1a (colour filled contours).

To check if there is a dependence of polarisation properties with energy, we used the same algorithm to calculate the PD and PA over a span of energy bins. The results can be seen in Fig. 1b, with the PA showing no apparent energy dependence. The PD shows a possible increase with energy, which we test in the following subsection.

During the *IXPE* observation, IGR J17091–3624 experienced a dip in the X-ray flux reaching as low as ~ 0.2 count s⁻¹ over all DUs, starting ~ 150 ks into the observation, and lasting for ~ 50 ks. We

https://heasarc.gsfc.nasa.gov/docs/ixpe/archive/

4 M. D. Ewing et al.

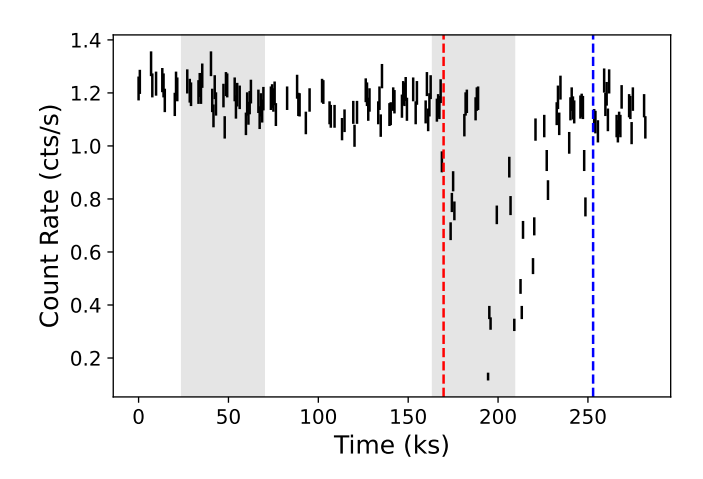


Figure 2. Light curve in counts per second of IGR J17091–3624 as observed by *IXPE* (black bars). The counts from each DU have been summed. The dip begins at the horizontal dashed red line, and ends at the horizontal blue dashed line. The shaded grey regions represent the two simultaneous *NuSTAR* observations. The error bars are derived from Poisson statistics.

plot the light curve of the total observation in Fig. 2, where the dip can clearly be observed. To test any effects that this may have on the observed polarisation, we calculated the polarisation properties excluding the events within the dip, again utilising the pcube algorithm. We found PD=8.4 \pm 1.8 per cent and PA=86° \pm 6°, which is consistent with the results calculated for the entire observation. We therefore conclude that due to the low number of counts contributed from the dip to the total observation, it does not have a significant effect on the observed polarisation.

3.2 Spectro-polarimetric analysis

Using XSPEC v12.14.1 (Arnaud 1996), we simultaneously fitted Stokes I,Q and U with several basic models representing different polarisation properties. The polarisation results and fit statistics for each model can be found in Table 1. We include a multiplicative constant component in each fit to account for cross-calibration between the DUs. We first fit the data with a model consisting of diskbb (Mitsuda et al. 1984) and powerlaw components, representing a multi-temperature black-body accretion disc and a power law with specific photon flux $\propto E^{-\Gamma}$. The interstellar absorption was accounted for using the model tbabs with the relative abundances from Wilms et al. (2000).

We first tested models with a constant, energy independent polarisation using model polconst (rows 2–3 in Table 1). For the model including both disc and powerlaw components, i.e. tbabs*polconst*(diskbb+powerlaw), we measure PD=7.6 \pm 1.8 per cent and PA= 84° \pm 7° with a fit statistic χ^2/d .o.f=1320/1334. This inferred polarisation is consistent with that measured using pcube, and we plot the resulting confidence contours in Fig. 1a (blue hollow contours).

We then fit the model without the diskbb component, i.e. tbabs*polconst*(powerlaw), which returned a fit statistic of χ^2 /d.o.f=1326/1334. We find that the polarisation properties between the two constant polarisation models are consistent, and that the disc is only detected in the flux spectrum with a statistical confidence of 1.8 σ according to an F-test. We plot the unfolded Stokes I, Q and U and the contributions to the fit statistic of the constant polarisation model excluding the disc component in Fig. 3.

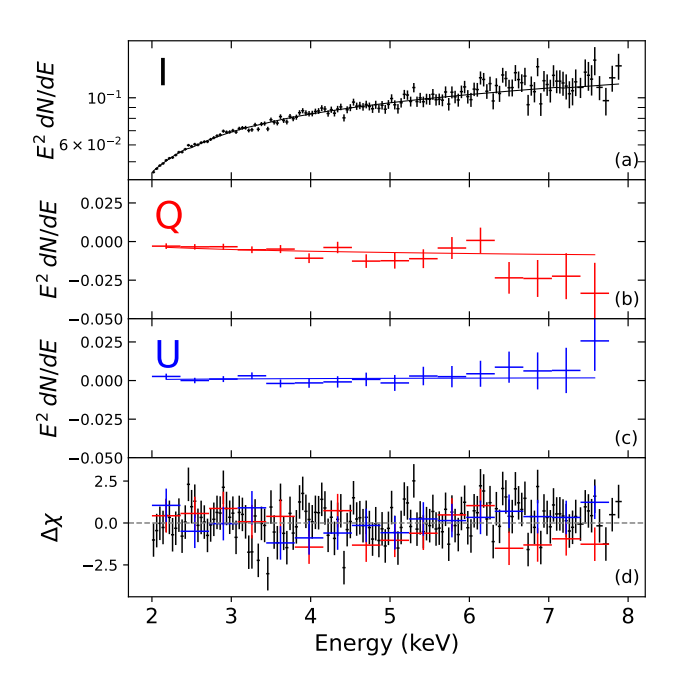


Figure 3. Spectral energy distribution of the constant polarisation model (row 3 of Table 1). For plotting purposes only, we group the three DUs and employ energy rebinning to achieve a target signal to noise of 6 by binning no more than 9 channels (i.e. the xspec command setplot rebin 6 9). (a) Best-fitting spectral model for Stokes I (black line) with unfolded data (black crosses). (b) Best-fitting spectral model (red line) with unfolded Stokes Q (red crosses). (c) Best-fitting spectral model (blue line) with unfolded Stokes U (blue crosses). (d) Contributions to fit statistic χ . dN/dE is in units of photons cm⁻² s⁻¹ keV⁻¹.

We then fit models to check for an energy dependence of the polarisation properties by replacing polconst with pollin, which assumes a linear dependence of PD and PA with photon energy (rows 3–5 of Table 1). The linear relationship is described as P(E) = $P_1 + (E/\text{keV} - 1) \times P_{\text{slope}}$ where P(E) is the energy dependent polarisation property (i.e. either PD or PA), P_1 is the polarisation property measured at 1 keV and P_{slope} is the gradient. We perform the fit under two different assumptions. The first assumption is that only the PD is variable with energy where the PA remains constant. This is achieved by freezing the slope parameter of PA to 0. In the second case, we assume that both PD and PA are energy dependent. We test these assumptions with (tbabs*pollin*(diskbb+powerlaw)) and without (tbabs*pollin*(powerlaw)) a disc component. We again find that the polarisation results are consistent between models with and without the diskbb component, and so from here we continue our analysis considering the simpler models containing only the powerlaw component.

To test if a polarisation linearly dependent on energy is preferred to a constant polarisation, we perform F-tests between the polconst model and the pollin model under the two aformentioned assumptions. The first test assuming only PD varies yields F=2.93, meaning the variable PD is only preferred by 1.7σ . Similarly for an F-test where PD and PA are free to vary, this model is only preferred to the constant polarisation model by 1.3σ . Although there is a hint of positive trending of PD with energy, no significant energy dependence of polarisation properties has been detected.

We note that, although the pcube and polconst measurements of PD are consistent within 1σ confidence, the polconst estimate

Model	PD (%)		PA (deg)		$N_{\rm H}~(10^{22}~{\rm cm}^{-2})$	Γ	kT _{bb} (keV)	χ^2 /dof
pcube	9.1 ± 1.6		83 ± 5		-	-	-	-
polconst*tbabs*(diskbb+po)	7.6 ± 1.8		84 ± 7		2.3 ^{+0.9} _{-0.8}	$1.56^{+0.15}_{-0.28}$	$0.48^{+0.51}_{-0.11}$	1320/1332
polconst*tbabs*po	7.6 ± 1.8		84 ± 7		1.39+0.15	1.58+0.04 -0.04	-	1326/1334
pollin*tbabs*(diskbb+po)	PD ₁ PD _{slope}	3^{+5}_{-3} $1.6^{+1.5}_{-1.6}$	PA ₁ PA _{slope}	84 ± 7 0.0	$2.0_{-0.7}^{+1.8}$	$1.52^{+0.18}_{-0.17}$	$0.54^{+0.47}_{-0.16}$	1318/1331
pollin*tbabs*po	PD ₁ PD _{slope}	3 ⁺⁵ 1.7 ^{+1.5} 1.1.6	PA ₁ PA _{slope}	84 ± 7 0.0	1.39 ^{+0.15} _{-0.15}	1.59+0.02 -0.04	-	1323/1333
pollin*tbabs*(diskbb+po)	PD ₁ PD _{slope}	3^{+5}_{-3} $1.8^{+1.4}_{-1.7}$	PA ₁ PA _{slope}	$90^{+10}_{-16} \\ -2^{+4}_{-3}$	$2.0^{+1.8}_{-0.7}$	$1.52^{+0.16}_{-0.17}$	$0.54^{+0.47}_{-0.16}$	1317/1330
pollin*tbabs*po	PD_1 PD_{slope}	3^{+5}_{-3} $1.8^{+1.4}_{-1.7}$	PA ₁ PA _{slope}	$90^{+17}_{-18} \\ -1.6^{+5.2}_{-1.6}$	$1.39^{+0.15}_{-0.15}$	$1.59^{+0.04}_{-0.04}$	-	1323/1332

Table 1. Model fitting results showing polarisation degree (PD), polarisation angle (PA), hydrogen column density ($N_{\rm H}$), power-law index (Γ), peak disc blackbody temperature ($kT_{\rm bb}$), and chi-square per degree of freedom (χ^2 /dof).

is systematically lower (see e.g. Fig. 1a). This is likely because the PD is increasing with energy, as has been observed for other higher signal to noise datasets (e.g. Ingram et al. 2024), and is hinted at here but with low statistical confidence. The polconst model has, by design, constant PD and so the best-fitting PD value is weighted towards the lower energies, for which there are more counts. The pcube algorithm, in contrast, calculates the polarisation properties averaged over the 2–8 keV bandpass (weighted by flux). To illustrate this, we plot in Fig. 1b the best-fitting PD and PA as a function of energy for our polconst (blue) and pollin (red) models. We see that, as expected, pollin agrees with the pcube points, whereas the polconst PD is slightly lower (whilst still within 2 σ uncertainties). We therefore adopt the pcube values as the best estimate of the 2–8 keV PD and PA.

3.3 State classification

For all models, we find that the hydrogen column density is in the range $N_{\rm H} \approx (1.4 - 2.3) \times 10^{22} \ {\rm cm}^{-2}$ (consistent with previous measurements; Wang et al. 2024) and the power-law index is $\Gamma \approx 1.6$ (see Table 1). These values are consistent with that seen in Wang et al. (2024). This photon index indicates that IGR J17091-3624 was in the hard state during the IXPE observation. To further consolidate the hard state classification, we also studied the timing properties. We created a light curve from all DUs with time bins of 1/256 s duration, and filtered the events such that they coincided with when all the DUs were in a good time interval (GTI). We then created a power spectrum averaged over a segment length of $T_{\text{seg}} = 64 \text{ s}$ using the STINGRAY python package (Huppenkothen et al. 2019). It is clear from Fig. 4 that a Type-C quasi-periodic oscillation (QPO) is present at ~ 0.2 Hz. Based on this combination of spectral and timing evidence, we conclude that the source is in a hard state and that the X-ray flux is dominated by the corona.

We also considered the *NuSTAR* observations taken during the *IXPE* exposure (see the grey shaded regions in Fig. 2). We find that the energy spectrum in the 3–79 keV *NuSTAR* energy range is dominated by the Comptonised emission, such that a disc component is not required to fit the spectrum. Figure 5 shows the results of fitting the combined spectrum of the two *NuSTAR* observations with the model tbabs * nthComp, where nthcomp is a thermal Comptonisation model (Zdziarski et al. 1996). We fix the hydrogen column density to $N_{\rm H} = 1.1 \times 10^{22}~{\rm cm}^{-2}$, the seed blackbody photon tem-

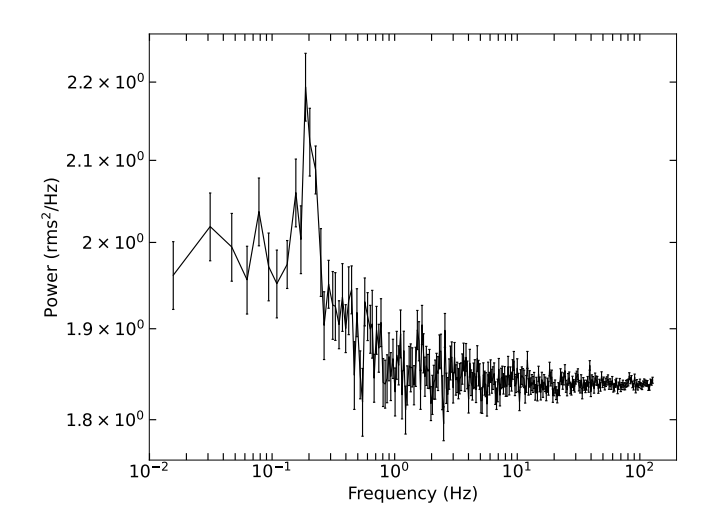


Figure 4. Power spectrum of the *IXPE* observation in the 2–8 keV band, calculated in fractional rms normalisation, where Poisson noise has not been subtracted. The input light curve was binned in 1/256 s time bins and the power spectrum was averaged over a segment size of 64 s. Logarithmic rebinning was applied (with the geometric rebinning parameter set to f = 0.2).

perature to $kT_{\rm bb} = 0.1$ keV, and the coronal electron temperature to $kT_e = 40$ keV. This electron temperature is motivated by preliminary fits, but we note that a reliable constraint on kT_e requires a very detailed analysis beyond the scope of this paper. The measured photon index of $\Gamma = 1.607 \pm 0.002$ is consistent with what we measure with IXPE (see Table 1). The residuals to this fit clearly reveal an iron line and Compton hump indicative of reflection. The presence of a clear Compton hump contributes to our hard state classification, since the Compton hump is much weaker than the iron line for a soft illuminating spectrum (García et al. 2022). The relative weakness of the reflection features (the residuals in the IXPE band are below 5 per cent) confirms that the 2-8 keV flux is dominated by Comptonised emission with a small (likely ~10-20 per cent based on preliminary fits) contribution from reflection. We leave a detailed spectro-polarimetric analysis jointly considering the IXPE and NuS-TAR observations for a follow up paper.

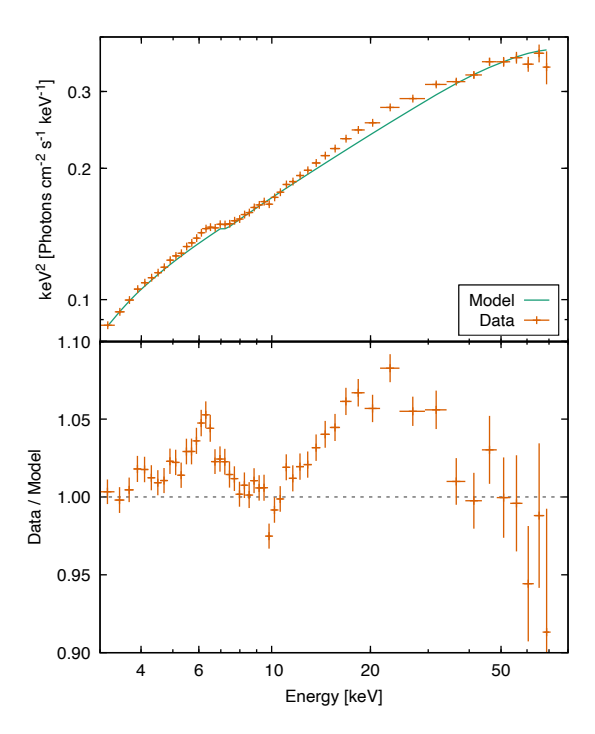


Figure 5. Unfolded *NuSTAR* energy spectrum fitted with the model tbabs*nthComp (top panel) and the corresponding residuals (bottom panel). FPMA and FPMB data are grouped for plotting purposes.

4 DISCUSSION

We have presented an IXPE observation of IGR J17091-3624 in the hard state and find that the 2–8 keV polarisation is PD = 9.1 ± 1.6 per cent and PA = $83^{\circ} \pm 5^{\circ}$. We are not able to compare the PA with the orientation of the jet in IGR J17091-3624 because it has never been spatially resolved by radio observations. Additionally, simultaneous MeerKAT observations do not significantly detect radio polarisation (Russell et al., in prep). As such, we are unable to make any inference on the relative orientation of the corona, but for the purposes of this discussion, we will assume that it is extended in the disc plane as is indicated by the polarisation aligning with the jet for all Xray polarisation detections of hard state BH XRBs and Seyfert-1 galaxies with resolved jets (Krawczynski et al. 2022; Gianolli et al. 2023; Veledina et al. 2023; Ingram et al. 2023). Simultaneous Very Large Telescope (VLT) optical polarimetric observations show an increasing PD with frequency $(2.9 \pm 0.5 \text{ and } 1.0 \pm 0.3 \text{ per cent in})$ the R and I bands, respectively; Baglio et al., in prep.), with a PA of $100^{\circ} \pm 5^{\circ}$ and $102^{\circ} \pm 8^{\circ}$, consistent with the *IXPE* PA within 2σ . This behaviour aligns with recent findings on BH XRBs in their hard state, where the optical PA has been observed to be similar to the PA in the X-rays, for example, in Cyg X-1 (Krawczynski et al. 2022; Kravtsov et al. 2023), Swift J1727.8-0127 (Veledina et al. 2023) and GX 339-4 (Mastroserio et al. 2025), and the position angle of the radio jet in V404 Cyg (Kosenkov et al. 2017) and MAXI J1820+070 (Veledina et al. 2019). Similarly, also for IGR J17091-3624 we favour a scenario in which the optical radiation originates in the outer regions of the disc and is polarised through Thomson scattering in the disc atmosphere or wind.

The observed 2–8 keV PD of ≈ 9 per cent is significantly higher than what has been measured thus far for other sources in corona-dominated states (e.g. ~ 4 per cent for both Cyg X-1 and Swift J1727–1613; Krawczynski et al. 2022; Veledina et al. 2023). Because the PD strongly depends on inclination, it is likely that

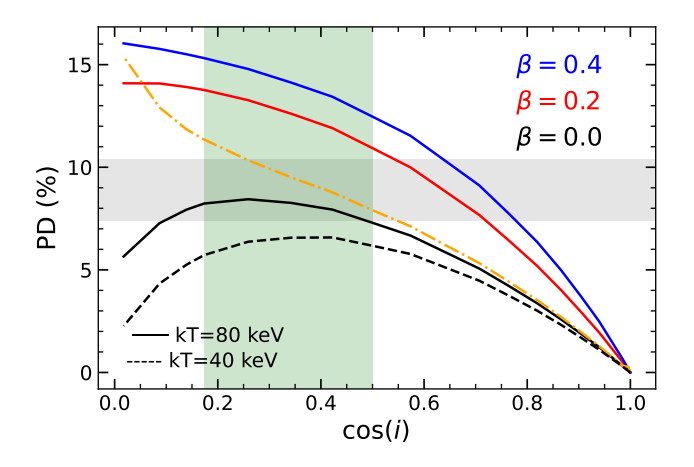


Figure 6. Predicted PD for a Comptonisation model in a slab-corona as a function of the cosine of the inclination for different bulk velocities. The black, blue and red lines represent bulk velocities of $\beta = v/c = 0, 0.2$ and 0.4, respectively. The solid and dashed lines correspond to coronal temperatures of $kT_e = 80$ and 40 keV, respectively. The orange dot-dashed line represents the PD influenced by scattering in a wind. The coronal optical depth was adjusted to produce spectral slope $\Gamma = 1.6$. The grey horizontal shaded area represents the limits on the observed PD measurement. The vertical green shaded region is the most likely range of inclination angles.

IGR J17091–3624 is more highly inclined than the other sources. However, the inclination of IGR J17091–3624 is not well constrained. Reflection spectroscopy modelling yields estimates of fairly low inclination ($i \sim 30^\circ - 40^\circ$; Xu et al. 2017), whereas the presence of dipping in the light curve (e.g. our Fig. 2 and Pahari et al. 2013) and wind signatures in the spectrum (Wang et al. 2024; Parra et al. 2024; Ponti et al. 2012), coupled with the absence of eclipses instead indicates that the inclination is in the range $60^\circ \le i \le 80^\circ$. The high amplitude of the Type-C QPO also points towards high inclination (Motta et al. 2015), consistent with the high inclination indicated by the high X-ray PD we observe here.

A PD of 9 per cent is high even for a high inclination source. To demonstrate this, we show in Fig. 6 the predicted PD as a function of inclination angle for a slab corona with seed photons provided from the side by a truncated disk (see Fig. 1c of Poutanen et al. 2023). This geometry is chosen to maximise the predicted PD (see Fig. 2 of Poutanen et al. 2023). We therefore note that these predictions should be seen as an upper limit of the expected PD, since any change to the assumed geometry (e.g. large coronal opening angles, significant inhomogeneities of the photosphere shape, etc.) would reduce the predicted PD. We use the analytic code compps (Poutanen & Svensson 1996; see also Veledina & Poutanen 2022) and assume a power-law index of Γ = 1.6 and a disc seed photon temperature of $kT_{bb} = 0.1$ keV (typical for the hard-state sources and optimal to maximise the PD). The grey shaded area represents the 1 σ confidence interval of the observed PD. The black lines represent the case where the electrons in the corona have no bulk velocity $(\beta = v/c = 0)$, only random thermal velocities. For the dashed line, we assume an electron temperature of $kT_e = 40$ keV, which is consistent with the fairly low value of kT_e yielded by our initial fits to the NuSTAR data. We see that the observed PD is above this line for all viewing angles. However, without a very detailed spectral analysis, $kT_{\rm e}$ is highly uncertain. We therefore also plot calculations assuming $kT_e = 80 \text{ keV}$ as solid lines, which maximises the predicted PD. We see that under this assumption, the $\beta = 0$ model is consistent with

the measured PD within uncertainties for inclinations in the range $60^{\circ} \le i \le 80^{\circ}$ as highlighted by the green shaded region.

A non-zero bulk outflow velocity, $\beta > 0$, of coronal electrons would increase the predicted PD due to relativistic aberration (Poutanen et al. 2023). We therefore plot examples of $\beta = 0.2$ and 0.4 in Fig. 6. We see that such values of the outflow velocity can reproduce the observed PD for much lower inclination angles. If the inclination of IGR J17091–3624 is $i \lesssim 60^\circ$ and the high PD results from bulk motion, this implies that other, higher inclination sources will be observed in future to have even higher PD.

Scattering in a disc wind adds another mechanism capable of affecting the polarisation properties (Tomaru et al. 2024; Nitindala et al. 2025), and IGR J17091–3624 is well known for strong wind signatures, albeit only in its exotic variability classes (Wang et al. 2024). The resulting PD depends on the optical depth of wind, its characteristic opening angle, angular distribution and polarisation of the incident X-ray emission. In Fig. 6 we show as the orange dot-dashed line an example for the PD boost by scattering in the wind for the case of incident radiation corresponding to Comptonization in the slab corona of $kT_e = 80$ keV producing a power-law spectrum with $\Gamma = 1.6$. We assumed the wind density profile following a Gaussian with opening angle $\alpha_{\rm W} = 20^{\circ}$ (Nitindala et al. 2025) and a mid-plane Thomson optical depth of $\tau_{\rm T} = 1$.

The same process could affect the optical polarisation as well. Our VLT polarimetric observations show an optical PD that increases slightly with frequency and a PA parallel to the X-ray PA measured with *IXPE*, suggesting that the polarisation originates from scattering within the plane of the accretion disc. This scattering could occur either in the atmosphere of the viscously heated optically thick accretion disc itself or in a disc wind, and distinguishing between these two scenarios is not possible. A more detailed analysis will be presented in a forthcoming paper focused on the optical polarisation properties of the source (Baglio et al. in prep.).

Reflection can also influence the observed PD, since the reflected emission can be more polarised than the directly observed coronal emission. The reflected emission is expected to be polarised perpendicular to the disc plane, thus aligning with the polarisation of the direct coronal emission (which we are assuming to align with the jet). In this case, the overall 2–8 keV PD is given by

$$PD = [(1 - R) \times PD_{cor}] + R \times PD_{ref}, \tag{1}$$

where R is the fraction of the 2–8 keV flux that is contributed by reflection, PD_{cor} is the PD of the corona and PD_{ref} is the PD of the reflection component. The maximum expected PD of the reflection component is ~ 20 per cent (Matt 1993; Poutanen et al. 1996; Podgorný et al. 2023), and a typical hard state 2–8 keV reflected fraction is $R \sim 0.1$ –0.2 (e.g. Krawczynski et al. 2022), which appears to be consistent with our NuSTAR data (Fig. 5). Therefore our observation of PD \approx 9 per cent gives a lower limit for the PD of the directly observed emission of PD_{cor} \gtrsim 6 per cent, which is still reasonably high compared with the expectations of thermal Compton scattering with no bulk velocity. More rigorous exploration of the physics of the corona will be provided by detailed spectro-polarimetric fits that jointly consider the *IXPE* and *NuSTAR* data, which we leave to future work.

5 CONCLUSIONS

We have obtained the first X-ray polarisation measurement for the BH XRB IGR J17091–3624. The time- and energy-averaged PD = 9.1 ± 1.6 per cent and PA = $83^{\circ} \pm 5^{\circ}$ (1σ errors) was measured

with statistical confidence 5.2σ using the model-independent pcube algorithm. We find no statistically significant dependence of the PD or PA on energy. From the shape of the energy spectrum, and the presence of a ~0.2 Hz Type-C QPO in the power spectrum, we confirm that the source was observed in the hard state where the X-ray flux is dominated by the corona. Without the orientation of the radio jet we cannot confirm the orientation of the corona with respect to the disc, but we do find that the X-ray PA is consistent with the I and R band polarization within 2 σ confidence, as has previously been found for other BH XRBs (Krawczynski et al. 2022; Mastroserio et al. 2025). The very high observed PD requires IGR J17091–3624 to have a favourable coronal geometry and to be viewed from a favourable angle for it to be explained by standard thermal Comptonisation models. If we are instead viewing from a lower inclination angle, the PD could have been boosted by the electrons in the corona having a mildly relativistic bulk outflow velocity, and/or by scattering in an optically thick disc wind. If this is true, we expect in future to observe other hard state BH XRBs with higher inclination angles that exhibit even higher PD.

ACKNOWLEDGEMENTS

M.E. and A.I. acknowledge support from the Royal Society. P.O.P. acknowledges financial support from the French Space National Agency (CNES) and the National Center of Scientifc Research (CNRS) via its "Action Thématique" PEM. T.D.R. and M.C.B. are INAF IAF research fellows. G.Mattand S.B. acknowledge financial support by the Italian Space Agency (Agenzia Spaziale Italiana, ASI) through the contract ASI-INAF-2022-19-HH.0. B.D.M. acknowledges support via a Ramón y Cajal Fellowship (RYC2018-025950-I), the Spanish MINECO grants PID2023-148661NB-I00, PID2022-136828NB-C44, and the AGAUR/Generalitat de Catalunya grant SGR-386/2021. M.D. and M.G. thank GACR project 21-06825X for the support and institutional support from RVO:67985815. The work of G.Matt and L.M. is partially supported by the PRIN 2022 - 2022LWPEXW - "An X-ray view of compact objects in polarized light", CUP C53D23001180006. A.V. acknowledges support from the Academy of Finland grant 355672. Nordita is supported in part by NordForsk.

DATA AVAILABILITY

IXPE data are publicly available from the HEASARC data archive (https://heasarc.gsfc.nasa.gov).

REFERENCES

Altamirano D., et al., 2011, ApJ, 742, L17

Arnaud K. A., 1996, in Jacoby G. H., Barnes J., eds, ASP Conf. Ser. Vol. 101, Astronomical Data Analysis Software and Systems V. Astron. Soc. Pac., San Francisco, pp 17–20

Baldini L., et al., 2022, SoftwareX, 19, 101194

Belloni T. M., 2010, in Belloni T., ed., Lecture Notes in Physics, Vol. 794, The Jet Paradigm - From Microquasars to Quasars. Springer Verlag, Berlin, pp 53–84, doi:10.1007/978-3-540-76937-8_3

Belloni T., Klein-Wolt M., Méndez M., van der Klis M., van Paradijs J., 2000, A&A, 355, 271

Beloborodov A. M., 1999, ApJ, 510, L123

Capitanio F., Del Santo M., Bozzo E., Ferrigno C., De Cesare G., Paizis A., 2012, MNRAS, 422, 3130

```
Costa E., Soffitta P., Bellazzini R., Brez A., Lumb N., Spandre G., 2001,
    Nature, 411, 662
Court J. M. C., Altamirano D., Pereyra M., Boon C. M., Yamaoka K., Belloni
    T., Wijnands R., Pahari M., 2017, MNRAS, 468, 4748
Dexter J., Begelman M. C., 2024, MNRAS, 528, L157
Done C., Gierlinski M., Kubota A., 2007, A&A, 15, 1
Eardley D. M., Lightman A. P., Shapiro S. L., 1975, ApJ, 199, L153
Esin A. A., McClintock J. E., Narayan R., 1997, ApJ, 489, 865
Fender R. P., Belloni T. M., Gallo E., 2004, MNRAS, 355, 1105
Galeev A. A., Rosner R., Vaiana G. S., 1979, ApJ, 229, 318
García J. A., Dauser T., Ludlam R., Parker M., Fabian A., Harrison F. A.,
    Wilms J., 2022, ApJ, 926, 13
Gianolli V. E., et al., 2023, MNRAS, 523, 4468
Gianolli V. E., et al., 2024, A&A, 691, A29
Haardt F., Maraschi L., 1993, ApJ, 413, 507
Harrison F. A., et al., 2013, ApJ, 770, 103
Huppenkothen D., et al., 2019, The Astrophysical Journal, 881, 39
Ingram A., et al., 2023, MNRAS, 525, 5437
Ingram A., et al., 2024, ApJ, 968, 76
Janiuk A., Grzedzielski M., Capitanio F., Bianchi S., 2015, A&A, 574, A92
Kosenkov I. A., Berdyugin A. V., Piirola V., Tsygankov S. S., Pallé E., Miles-
    Páez P. A., Poutanen J., 2017, MNRAS, 468, 4362
Kravtsov V., et al., 2023, A&A, 678, A58
Krawczynski H., Beheshtipour B., 2022, ApJ, 934, 4
Krawczynski H., et al., 2022, Science, 378, 650
Kuulkers E., Lutovinov A., Parmar A., Capitanio F., Mowlavi N., Hermsen
    W., 2003, The Astronomer's Telegram, 149, 1
Malzac J., Belmont R., 2009, MNRAS, 392, 570
Marinucci A., et al., 2022, MNRAS, 516, 5907
Markoff S., Nowak M. A., Wilms J., 2005, ApJ, 635, 1203
Mastroserio G., et al., 2025, ApJ, 978, L19
Matt G., 1993, MNRAS, 260, 663
Miller-Jones J. C. A., et al., 2021, Science, 371, 1046
Mitsuda K., et al., 1984, PASJ, 36, 741
Motta S. E., Casella P., Henze M., Muñoz-Darias T., Sanna A., Fender R.,
    Belloni T., 2015, MNRAS, 447, 2059
Nitindala A. P., Veledina A., Poutanen J., 2025, A&A, 694, A230
Novikov I. D., Thorne K. S., 1973, in Witt B., Witt C., eds, Black Holes (Les
    Astres Occlus). Gordon & Breach, New York, pp 343-450
Pahari M., Yadav J. S., Rodriguez J., Misra R., Bhattacharyya S., Pandey
    S. K., 2013, ApJ, 778, 46
Parra M., Petrucci P. O., Bianchi S., Gianolli V. E., Ursini F., Ponti G., 2024,
    A&A, 681, A49
Podgorný J., et al., 2024, A&A, 686, L12
Podgorný J., Dovčiak M., Goosmann R., Marin F., Matt G., Różańska A.,
    Karas V., 2023, MNRAS, 524, 3853
Ponti G., Fender R. P., Begelman M. C., Dunn R. J. H., Neilsen J., Coriat M.,
    2012, MNRAS, 422, L11
Poutanen J., Svensson R., 1996, ApJ, 470, 249
Poutanen J., Vurm I., 2009, ApJ, 690, L97
Poutanen J., Nagendra K. N., Svensson R., 1996, MNRAS, 283, 892
Poutanen J., Krolik J. H., Ryde F., 1997, MNRAS, 292, L21
Poutanen J., Veledina A., Zdziarski A. A., 2018, A&A, 614, A79
Poutanen J., Veledina A., Beloborodov A. M., 2023, ApJ, 949, L10
Schnittman J. D., Krolik J. H., 2010, ApJ, 712, 908
Shakura N. I., Sunyaev R. A., 1973, A&A, 24, 337
Sunyaev R. A., Titarchuk L. G., 1985, A&A, 143, 374
Svensson R., Zdziarski A. A., 1994, ApJ, 436, 599
Svoboda J., et al., 2024, ApJ, 966, L35
Tomaru R., Done C., Odaka H., 2024, MNRAS, 527, 7047
Ursini F., Matt G., Bianchi S., Marinucci A., Dovčiak M., Zhang W., 2021,
    MNRAS, 510, 3674
Veledina A., Poutanen J., 2022, Polarization of Comptonized emission in slab
    geometry, doi:10.5281/zenodo.7116125
Veledina A., Poutanen J., Vurm I., 2011, ApJ, 737, L17
Veledina A., et al., 2019, A&A, 623, A75
```

```
Weisskopf M. C., et al., 2022, JATIS, 8, 026002
Wilms J., Allen A., McCray R., 2000, ApJ, 542, 914
Wood C. M., et al., 2024, ApJ, 971, L9
Xu Y., et al., 2017, ApJ, 851, 103
Zdziarski A. A., Johnson W. N., Magdziarz P., 1996, MNRAS, 283, 193
This paper has been typeset from a TFX/IATFX file prepared by the author.
```

Veledina A., et al., 2023, ApJ, 958, L16 Wang J., et al., 2024, ApJ, 963, 14